Pulsed laser damage resistance of nano-structured polarizers for 1064nm

Douglas S. Hobbs*, Bruce D. MacLeod, Anthony D. Manni, and Stephen M. Consoles
TelAztec LLC, 15 A Street, Burlington, MA, USA 01803-3404

ABSTRACT

Non-diffracting surface relief grating structures combined with high refractive index films were designed as high efficiency, narrow-band, polarization selective high reflectors for the near infrared wavelength region. Such nano-structure polarizers (NSP) have the potential for increased laser damage resistance due to reduced absorption and the ability to create arbitrary refractive index layers with fewer defects and reduced electric field enhancement. Three NSP designs based on gratings in fused silica combined with tantala and magnesium fluoride films, were prototyped and characterized for efficiency, surface absorption and pulsed laser damage resistance at a wavelength of 1064nm. Most NSP prototypes exhibited >99.7% reflectivity for linearly polarized illumination over a several nm bandwidth with high transmission of the orthogonal polarization leading to extinction ratios greater than 300:1 for the best performers. NSP prototype performance was worse than predicted by the design models due to the imprecise replication of the fused silica grating surface in the film layers resulting from the deposition system configuration. Surface absorption measurements showed the expected low absorption in the 4 ppm range for film layers deposited on non-structured control substrates, but voids and growth defects revealed through scanning electron microscopy in the same films deposited over gratings, likely caused an observed 5 fold increase in NSP prototype surface absorption. Initial 1064nm wavelength, 6.2ns pulsed laser damage testing also showed a reduced damage resistance for NSP prototypes compared to the films deposited on non-structured control substrates. Follow-on work to eliminate the film defects for NSP designs is underway.

Keywords: Nano-Texture, Micro-Structured High Reflector, Guided Mode Resonant Mirror, Pulsed LiDT, High Energy Lasers, RAR, Surface Structure Resonance, Polarizer Optic

1.0 INTRODUCTION

Adding optical functionality to the surfaces of optics using arrays of sub-wavelength sized structures offers many advantages over conventional thin-film interference coatings. For example the creation of anti-reflecting (AR) surfaces such as the periodic Motheye texture or the carpet-like Random AR (RAR) texture, yields a surface with zero added absorption and a laser damage resistance many times higher than any type of thin-film coating deposited by any method[1-6]. Partial reflectors, waveplates, diffraction gratings, and even some filter functions can all be constructued from micro-meter or nano-meter scale surface relief features to yield robust and reliable optics with stable performance over long operational times. Steady progress over recent years has been made in demonstrating these same performance benefits in microstructure based filter and high reflector (HR) designs[6-10]. Highly efficient narrow-band micro-structure HR prototypes with uniform properties over large areas have been realized, such as the 5cm diameter filter shown on the right. However, the goal of increased laser damage resistance for very high efficiency nano-structure resonant (NSR) filters, polarizers and high reflectors has yet to be realized. In this study, work reported previously for nano-structure polarizers (NSP) designed for near UV laser applications[11], is continued for NSP devices operating on near infrared (NIR) wavelength lasers. Multiple NSP designs were explored and a matrix of variants were fabricated, the structure cross sections analyzed, and then characterized for surface absorption and pulse laser damage resistance.

* dshobbs@telaztec.com; phone 1-781-229-9905; www.telaztec.com

Laser-Induced Damage in Optical Materials 2018: 50th Anniversary Conference, edited by Christopher Wren Carr, Gregory J. Exarhos, Vitaly E. Gruzdev, Detlev Ristau, M.J. Soileau, Proc. of SPIE Vol. 10805, 108051E

2.0 NSP DESIGN MODELS

An interesting NSP function can be designed that combines broad-band HR centered at a wavelength of 1064nm for one polarization state, narrow-band HR at a wavelength of 1030nm for the orthogonal polarization state, and high performance AR near the resonant bands. To realize an NSP structure that can be fabricated easily, the model is constrained to materials with well-known optical properties, and to in-house fabrication methods. Figure 1 shows diagrams of three NSP designs that can be created by etching a simple binary grating into the surface of a substrate such as fused silica (refractive index n_s 1.44 at 1064nm), and subsequently depositing one or two layers of thin-films onto the grating in a manner that replicates the grating in the film layers. Tantalum pentoxide (Ta_2O_5, light green) with refractive index n_2 of 2.08 at 1064nm, and magnesium fluoride (MgF_2, pink) with refractive index n_1 of 1.38, were chosen as high and low index materials respectively due to their low absorption properties and wide availability. A three level structure is created with two film layers in the NSP1 and NSP2 designs where the impact on surface absorption and laser damage resistance can be observed relative to deposition order. The NSP3 design adds a fourth level in order to expand the predicted performance bandwidth.

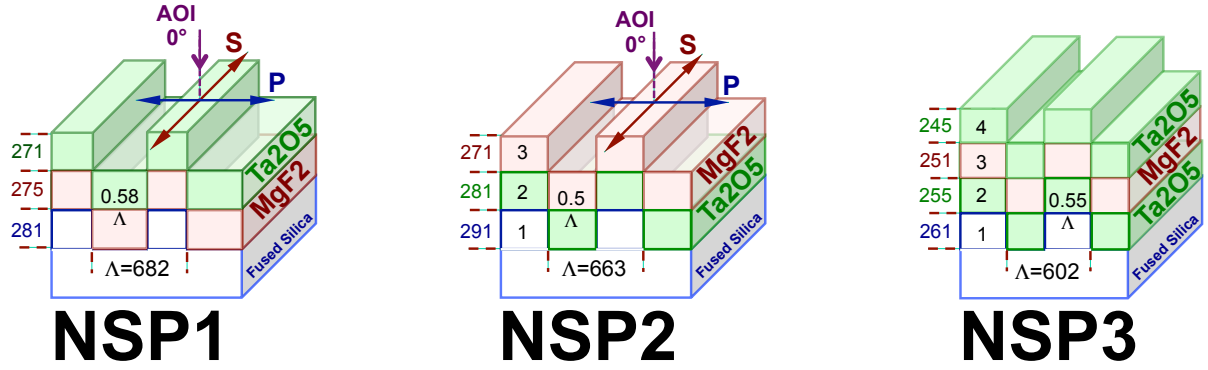

Figure 1: Diagrams of the three dimensional NSP structure variants input to the RCWA modeling software.

2.1 Rigorous Coupled Wave Analysis (RCWA) modeling for NSP Design[12]

Figure 2 gives the predicted reflection (left axis) from an NSP2 structure for normal incidence light polarized parallel to the grating lines ('S', transverse electric, solid red curve), or polarized perpendicular to the grating lines ('P', transverse magnetic, solid blue curve). A reflection above 99.7% is predicted for a 5nm bandwidth centered at 1064nm for S-polarized illumination. Another efficient resonance is predicted for P-polarized light near 1030nm. The design has high transmission (good AR) for the 1040-1075nm range, and the polarization contrast, defined as the ratio of S-polarized light reflection to P-polarized light reflection (S/P, dashed black curve, Extinction Ratio, right axis), is predicted to be greater than 5000:1 at 1064nm with a 1000:1 bandwidth of 30nm. This contrast makes the design commercially valuable as a polarizing high reflector.

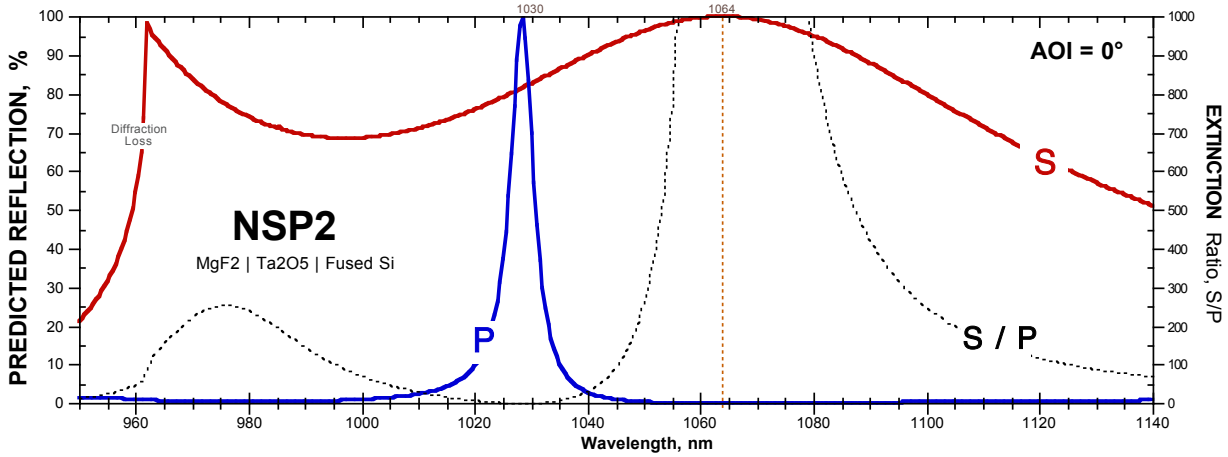

Figure 2: Predicted spectral reflection of S- (red) & P-polarized light (blue) from a 3-level NSP2 filter model.

Figure 3 shows the predicted reflection from a 4 level NSP3 structure consisting of a 602nm pitch binary profile grating etched 261nm deep in a fused silica substrate and then coated with Ta_2O_5 and MgF_2 as shown on the right in Figure 1. Structure parameters (pitch, duty cycle, and film thicknesses) where optimized for a reflectance maximum at 1064nm for S-Polarized light (solid red curve), with good AR properties in the NIR band for P-Polarized light (solid blue curve). Adding the third film layer increases the 99.7% bandwidth to nearly 25nm, five times larger than the 3 level NSP2 design, with minimal increase in surface absorption. In addition, the NSP3 reflective polarizer design operates over a nearly 200nm range in the NIR at an extinction ratio (dashed black curve, right axis) greater than 100:1.

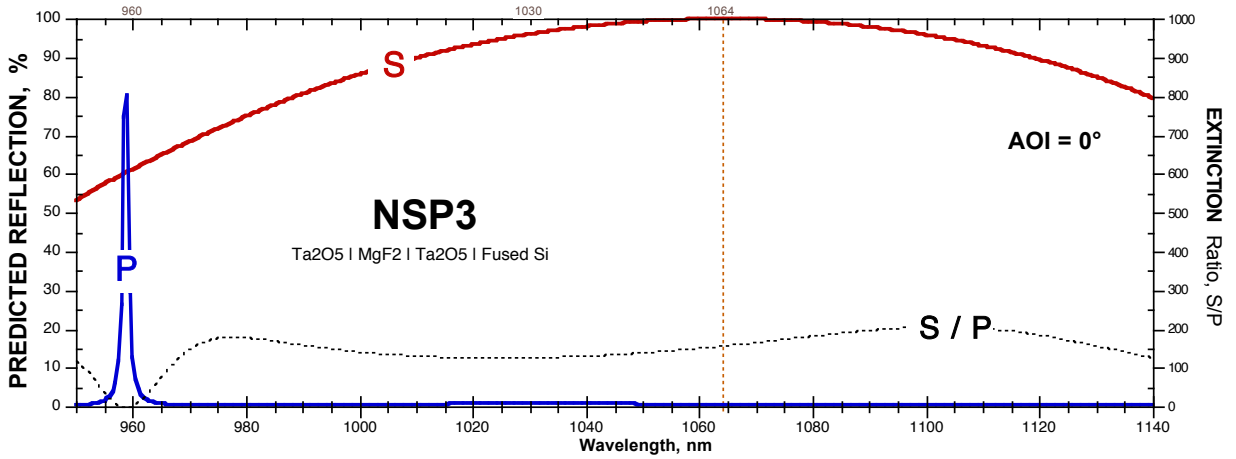

Figure 3: Predicted spectral reflection of S- (red) & P- polarized light (blue) from a 4-level NSP3 filter model.

2.2 Electric Field Intensity Distribution Models for NSP Design

Understanding the distribution of, and then minimizing, the electric field intensity (EFI) within the resonant structure of an NSP design, should yield higher laser damage resistance. Calculating EFI has long been a powerful tool available to designers of 2D multi-layer thin-film interference coating stacks, but the calculation power needed for simulating 3D structures has only recently become practical and available. Using the COMSOL Multiphysics software[13], the NSP2 design was input and the software iterated until the predicted spectral reflection and transmission values matched the RCWA model predictions. Spatial maps of the EFI then showed peak regions within the NSP2 grating structure where damage is likely to originate. Figure 4 shows these single wavelength EFI maps for the NSP2 design where the color scale runs from blue at the lowest intensity to dark red as the highest intensity. The different material regions are labeled. Notice the peak intensity for the 1064nm S-Polarization resonance shown by map a) on the left is located at the top of the grating lines split between high and low refractive index materials. Map b) shows a greatly reduced EFI for S-Polarized light at a longer wavelength off the resonant peak. Even greater EFI is seen for the P-Polarization resonance at 1028nm, but the EFI distribution is more uniform across the unit cell. By changing the shape and composition of the features in the resonant array, the peak EFI can be minimized and spread out over a greater volume, leading to increased damage resistance.

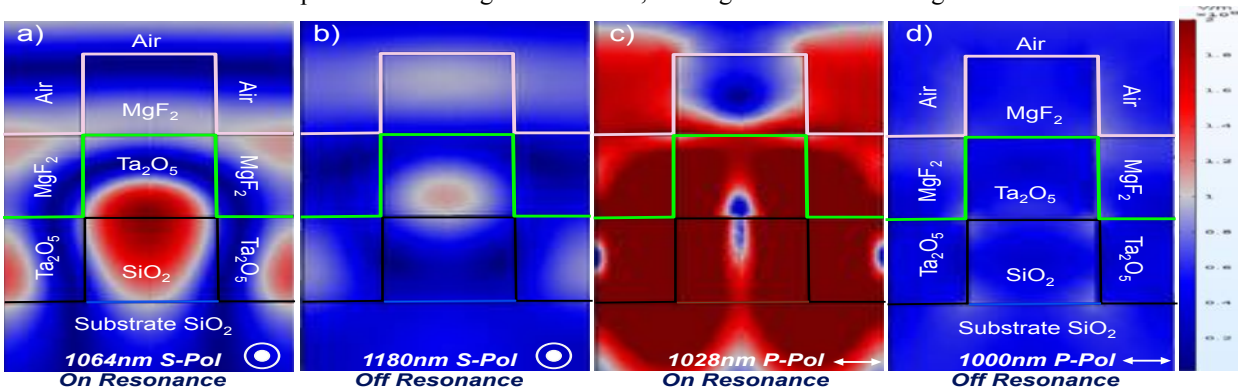

Figure 4: EFI maps of NSP2 design filters on and off the resonant peaks using S- and P-polarized illumination.

3.0 NSP FABRICATION AND MEASURED PERFORMANCE

Prototypes of all three NSP designs shown in Figure 1 were fabricated on laser quality polished round UV fused silica (Corning 7980 Grade 0A) windows, 25.4mm diameter, 4mm and 1mm thick. The NSP fabrication sequence begins with pattern origination in a sacrificial mask material using holographic or interference lithography[14] (IL), followed by reactive ion etching (RIE) to transfer the mask pattern into the fused silica surface, then finishing with the deposition of the film layers. Characterization of the prototypes was done through spectral reflection and transmission measurements, spectroscopic ellipsometry[15] to measure the deposited film refractive index, Common-Path Photo-Thermal Interferometry[16] (CPPI) to measure the bulk and surface absorption, scanning electron microscopy (SEM) to analyze the NSP structure, and finally standardized pulsed laser induced damage threshold (LiDT) testing to determine the NSP damage resistance relative to control samples.

3.1 Nano-structure polarizer prototype fabrication.

The beam from a blue (λ=457nm) frequency doubled DPSS laser was employed in the "Littrow", or "folded-mirror" IL configuration to originate the NSP grating patterns. Micrometers on the mirrors in the IL system allow fine tuning of the grating pitch to the NSP1, NSP2, and NSP3 targets of 683, 663, and 602nm. Pattern pitch is measured optically using white light delivered and returned at the Littrow angle through a bifurcated fiber reflection probe with spectrometer readout. Prototypes were then prepared by spin coating photoresist on the fused silica windows to a thickness that is anti-reflecting at the blue laser wavelength and incident angle in the IL system. Patterning contrast is high in an IL system as can be seen by the scanning electron microscope (SEM) images taken of an initial NSP1 calibration sample shown in Figure 5.

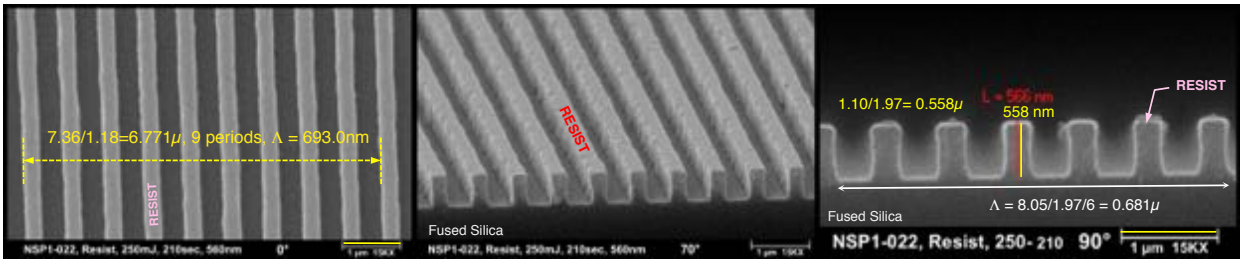

Figure 5: Overhead (0°), elevation (70°), and profile (90°) SEM views of grating lines defined in photoresist on fused silica.

Next RIE with fluorine-based gases transfers the IL generated photoresist gratings into the fused silica surfaces. A Trion Technologies Phantom II etch tool with a secondary inductively coupled plasma (ICP) generator was used in a low pressure, high density process for highly selective etching of fused silica. Figure 6 shows the clean uniform gratings in fused silica resulting from this RIE/ICP process. The top row of SEM images in the figure show the grating patterns after etch but before removal of the residual photoresist mask material. From these SEMs and the images of the stripped fused silica surfaces (bottom set), the etch rates of both the photoresist mask material and the fused silica substrates was determined to be about 64 and 56nm/min respectively for a selectivity about 0.9.

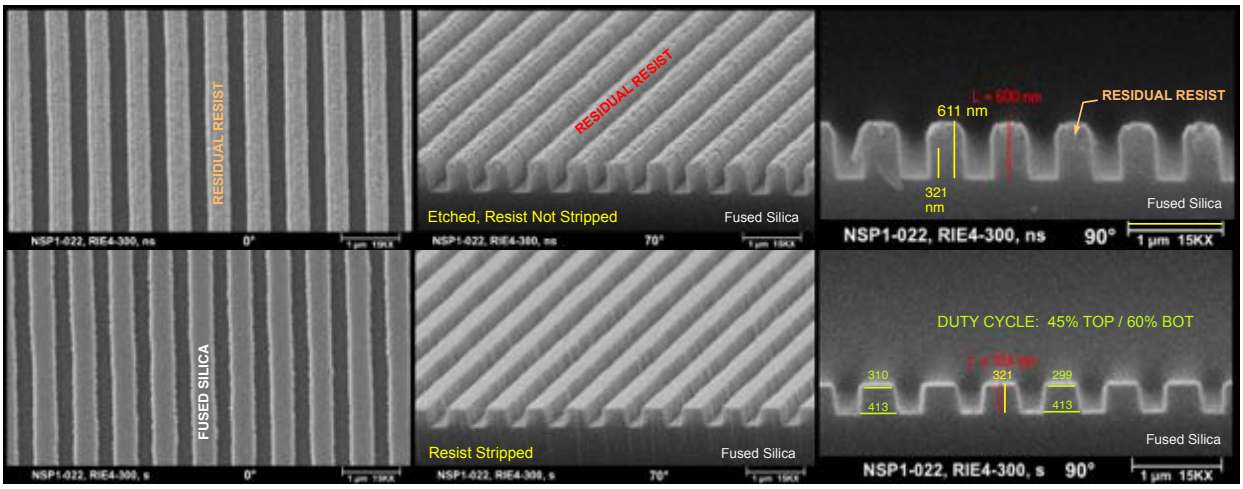

Figure 6: RIE process, SEM views of grating lines etched in fused silica before (top) and after (bot) removal of residual resist.

Using optimized IL and RIE processes, a matrix of over 30 fused silica windows was prepared that consisted of three sets of NSP based designs with grating depth and duty cycle as variants in each set. All three sets were then shipped to Quality Thin Films (QTF) of Oldsmar Florida for thin-film deposition by e-beam evaporation. The first run for the NSP1 design calls for a coating of MgF_2 first with a Ta_2O_5 top layer. The NSP2 set is the same two-materials but with Ta_2O_5 first and MgF_2 on top. Last the NSP3 set is 3 layers, Ta_2O_5-MgF_2-Ta_2O_5. In each set were included thin fused silica grating samples for SEM analysis, and thick fused silica windows that are suitable for pulsed laser damage testing, spectroscopic ellipsometry, and for surface absorption measurements. As-polished (no grating) windows were also included as controls for all subsequent measurements.

Silicon wafers were included in the film deposition runs by QTF to facilitate optical constant measurements, to evaluate the film roughness, and to allow verification of the film thickness as-deposited. Figure 7 shows SEM images of a cross-section of the NSP1 witness wafer. The Ta_2O_5 top layer appears brighter than the MgF_2 bottom layer indicating a lower packing density – larger columnar growth with a corresponding roughness on the surface. Imaging of NSP2 wafers are consistent with a darker, more dense, smoother MgF_2 top layer and a brighter Ta_2O_5 bottom layer. Film thickness measurements show no more than 2% deviation from the target thickness.

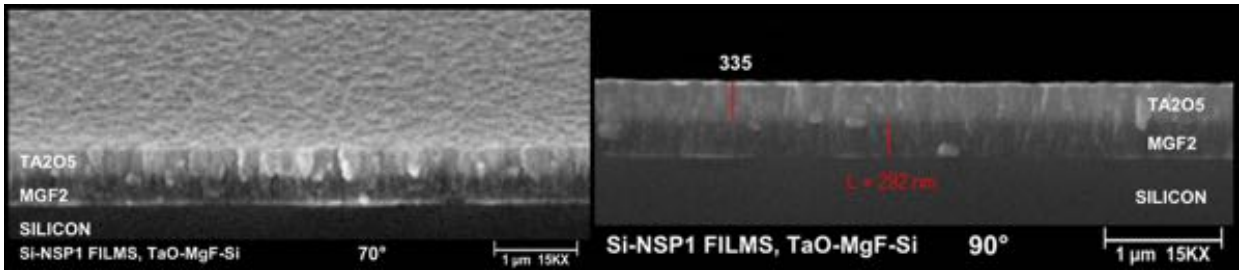

Figure 7: SEM views (70° elevation, 90° profile) of NSP1 design film layers deposited by QTF on a silicon witness wafer.

The structure input to the RCWA modeling software for the NSP designs is a binary structure with the films replicating the grating profile. This stepped profile was unlikely to be matched exactly for typical film deposition methods. Modeling where a sloped sidewall angle of the grating resulting in a sloped sidewall angle within the films showed only minor impact on the predicted performance. Figure 8 shows the concept. It is expected that evaporation methods with low divergence of the matter stream would lead to a close approximation of the model structure. However, if the deposition apparatus allowed a non-radial, high divergence matter stream, the resulting film structure would show voids and variable duty cycle due to growth from the edges of the grating lines and shadowing in the grating valleys as shown on the right side of Figure 8. Models with such structure defects show split resonances and poor AR properties outside the resonant band.

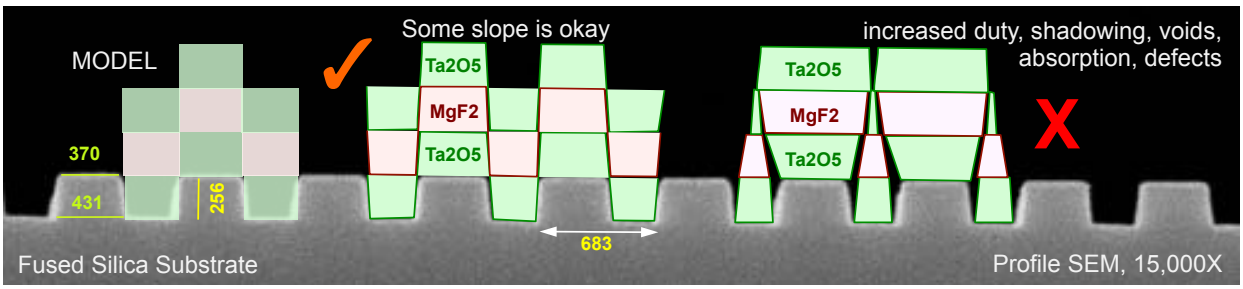

Figure 8: Graphic illustrating how thin-films could deposit on a grating surface using an NSP1 sample SEM profile (90°).

Unfortunately the films deposited over grating surfaces do not stack up in the binary – or even sloped binary – fashion needed to match the model predicted performance. Figure 9 shows SEM cross sections of NSP1 and NSP2 prototypes where the Ta_2O_5 layers again appear brighter and more rough than the MgF_2 layers. It also appears that a significant deposition angle caused shadowing in the valleys and rounding of the edges to such an extent as to nearly fill-in the valleys at the top surface. Voids where the triangular growth in the valleys meets the rounded overfill on the top of the grating lines may also lead to increased surface absorption and lower damage resistance. These results are being discussed with QTF to determine how the evaporation tooling and procedure can be modified for a more radial, less divergent deposition.

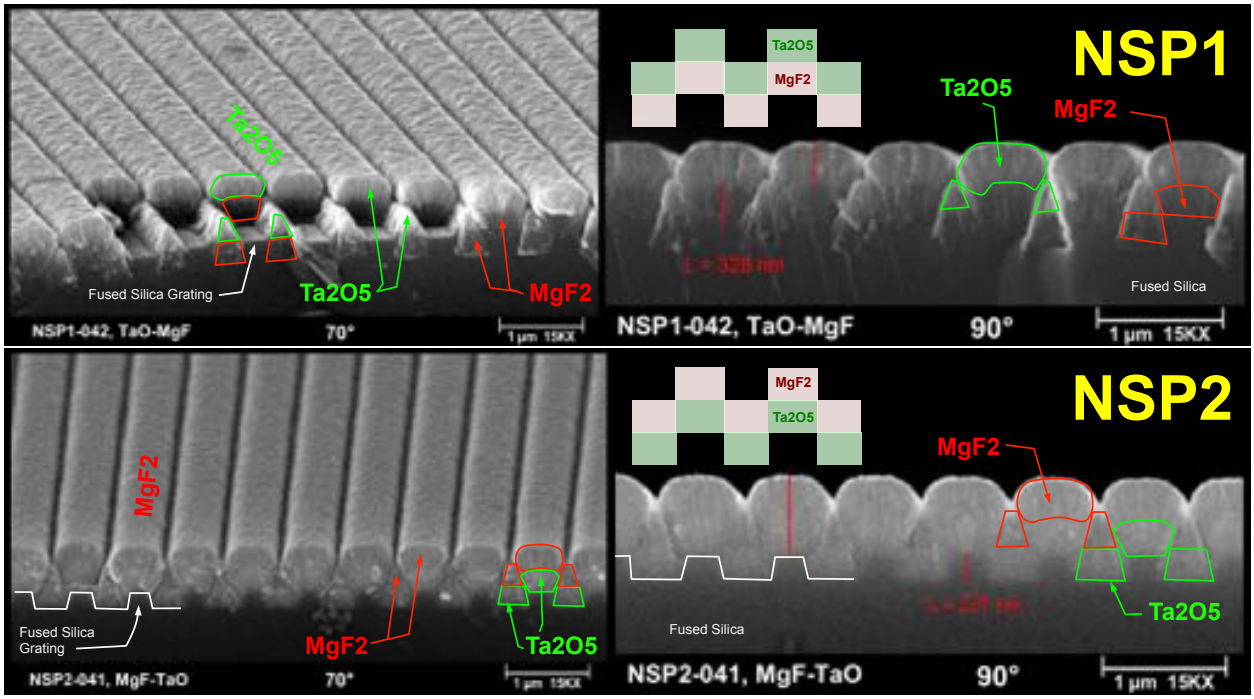

Figure 9: Two-layer deposition by evaporation. 70° and 90° SEM views of grating lines etched in fused silica after deposition of MgF_2 topped with Ta_2O_5, NSP1 (top), and an NSP2 grating after deposition of Ta_2O_5 topped with MgF_2 (bot).

3.2 Spectroscopic Ellipsometry

Witness silicon wafers for the Ta_2O_5 and MgF_2 films deposited by QTF were sent to J.A. Woollam for spectroscopic ellipsometry measurements that give the film optical constants - refractive index n and absorption coefficient k - as a function of wavelength. At near infrared wavelengths the measurement recorded k values of zero for both films, which is consistent with the literature. For refractive index n, the measured values are shown in Figure 10 along with diagrams of the witness wafers for each of the NSP1, NSP2, and NSP3 prototype film deposition runs. The green lines at the top of the plot show the refractive index measured for the Ta_2O_5 films, while the red curves at the bottom show the MgF_2 index. Numerical values for the refractive index at 1064nm are given as labels for each curve. A refractive index of 1.373 is found for MgF_2 deposited on the NSP1 and NSP3 wafers, closely matching the expected values. A slightly lower index of 1.36 was measured for the NSP2 MgF_2 film, a result which may be within the error of the measurement.

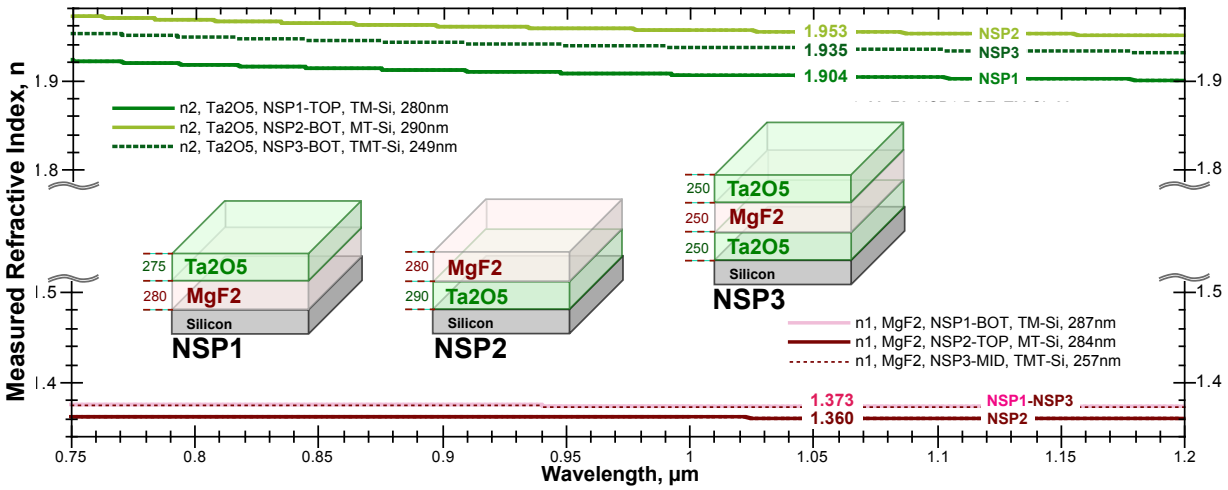

Figure 10: Measured refractive index of Ta_2O_5 (green curves) and MgF_2 (red curves) deposited on NSP1-2-3 witness wafers.

The expected and literature value for the refractive index of Ta_2O_5 is 2.085 at 1064nm. All of the NSP models have used this value. The ellipsometry measurements show a significantly lower refractive index around 1.935 that varies depending on the deposition order and number of layers. While some variation was expected, the low refractive index was not, and both need to be accounted for in the NSP design models.

To see the effect of the lower Ta_2O_5 refractive index on the predicted performance, the NSP2 design model was modified to replace the Ta_2O_5 layer with hafnium oxide (HfO_2) which happens to have a refractive index of 1.93, a match to the measured Ta_2O_5 index. Figure 11 shows the predicted reflection from the NSP2 structure using HfO_2 (solid red and blue curves), compared to the original prediction (dashed red and blue curves). The resonant peak is seen to shift to shorter wavelengths for both S- and P-polarized illumination, and the bandwidth of the resonance has decreased. In addition, the lower refractive index leads to higher reflection outside the resonant band with the corresponding decrease in polarization contrast.

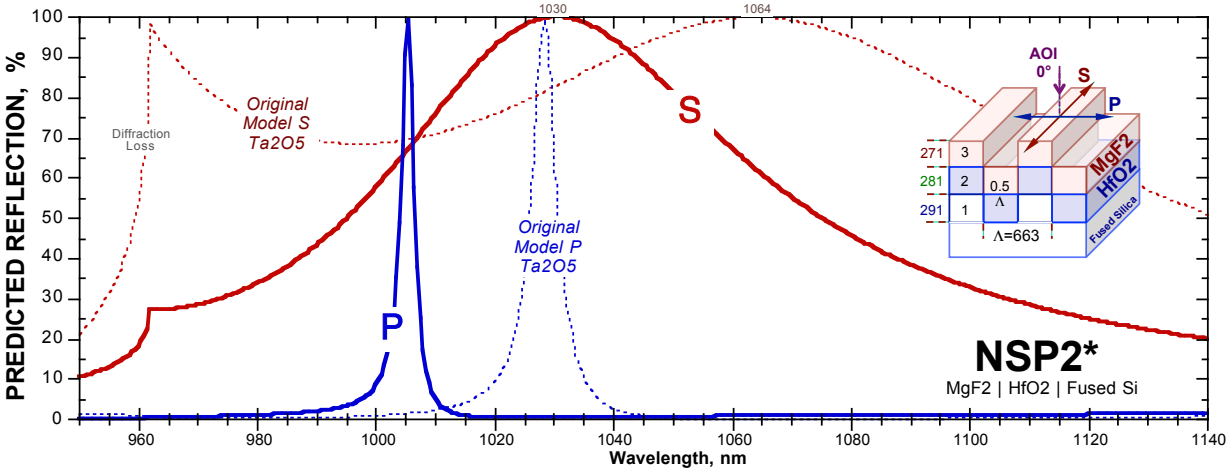

Figure 11: Predicted spectral reflection of S- (solid red) & P-polarized light (solid blue) from a revised NSP2 design based on a reduced refractive index for the Ta_2O_5 layer (HfO_2, n=1.93), compared to the original NSP2 model (n=2.08, dashed curves)

3.3 Spectral Reflection Measurements

The problems of film stack up (Fig. 9) and the lower than expected refractive index of the Ta2O5 layers, cause a deviation of the measured NSP prototype performance from the model predictions. Figure 12 shows the measured on-axis spectral reflection from prototype number 099 of the NSP2 design. Solid color curves show the measured S- and P- polarized light response in comparison with the dashed curves showing the original NSP2 model prediction. A maximum efficiency reflection for S-polarized light is observed centered at 1076nm, just off the 1064nm target, while the response to P-polarized light is split and low efficiency near the target of 1030nm. Note that the high measured transmission of P-Polarized light combined with the peak efficiency resonance found for S-Polarized light, make the Figure 12 NSP2 prototype a useful polarizer with greater than 300:1 extinction ratio (dashed black curve and right hand axis) at 1064nm, and >100:1 ratio from 1040nm to 1100nm.

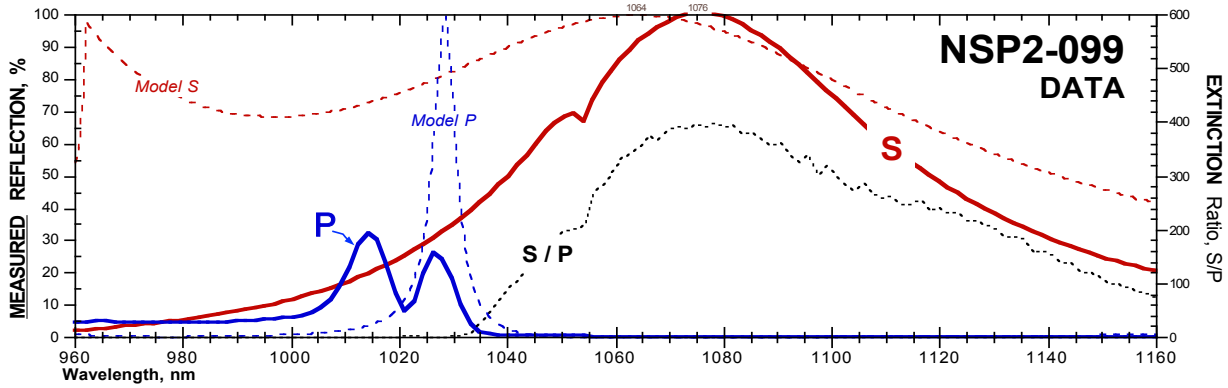

Figure 12: Measured spectral reflection of S- (solid red) & P-polarized light (solid blue) from NSP2 prototype # 099.

Figures 13 and 14 show the measured spectral reflection of NSP1, NSP2, and NSP3 prototypes respectively (solid red and blue curves), each compared to re-iterated design models incorporating HfO_2 in place of Ta_2O_5 to account for the lower measured Ta_2O_5 refractive index (dashed red and blue curves). Given again in each figure is the polarization extinction ratio indicated by the dotted black curves corresponding to the right-side axis. Figure 13 shows a much better fit of the measured S-polarized reflection to the re-iterated model prediction. The relationship between the S- and P-polarized reflections is generally the same as the revised model, except for the split and shifted P-polarized resonance as well as the slight notch in the S-polarized reflection. These spectral features likely arise from the non-ideal film layer overlap and resulting structure deviation from the model binary structure. The same analysis applies to the NSP3 prototype data of Figure 14.

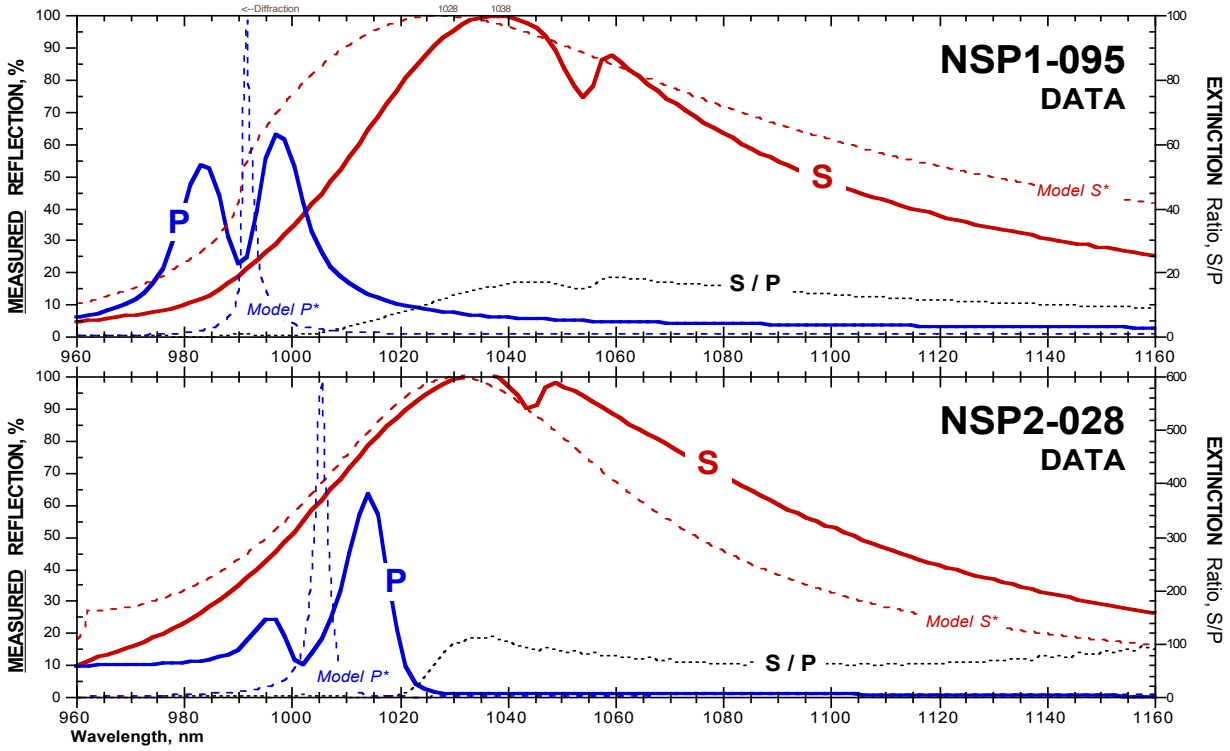

Figure 13: Measured spectral reflection of S- (solid red) & P-polarized light (solid blue) from NSP1 (top) and NSP2 (bot) prototypes compared to revised models (dashed curves) with reduced refractive index for the Ta_2O_5 layer (HfO_2, n=1.93).

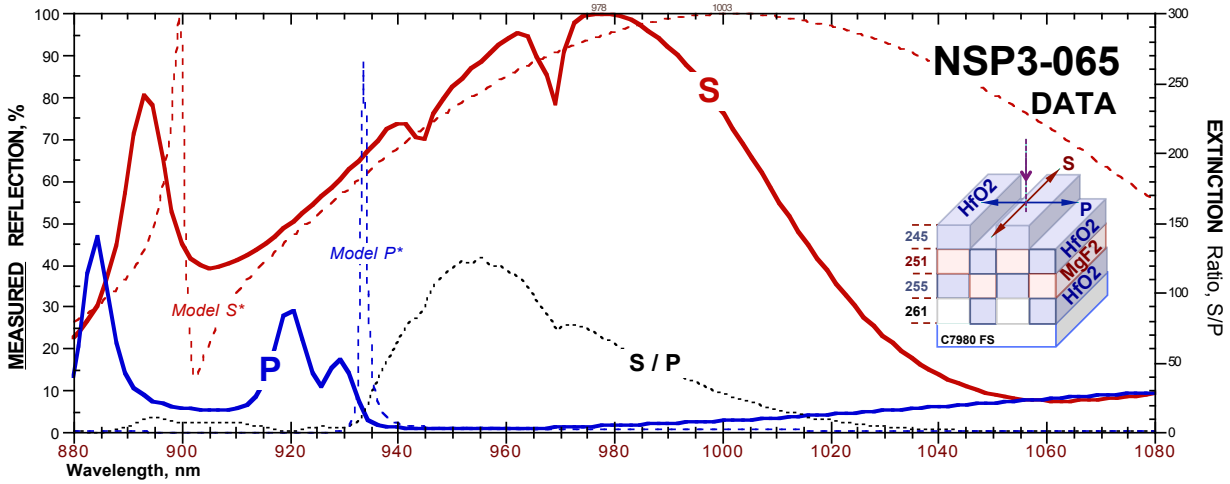

Figure 14: Measured spectral reflection of S- (solid red) & P-polarized light (solid blue) from an NSP3 prototype compared to a revised NSP3 model (dashed curves) with reduced refractive index for the Ta_2O_5 layer (HfO_2, n=1.93).

3.4 Surface Absorption Measurements

Absorption at the surface of an optic operating in a high power laser system is strongly correlated with laser damage resistance. A primary potential advantage of NSR technology over multi-layer dielectric thin-film HR, is the greatly reduced surface absorption for the one or two material layers in the NSR structure compared to the 20-50 layers in a typical HR film stack. A highly sensitive method for measuring absorption to the part per million (ppm) level is know as Common-Path-Photothermal-Interferometry (CPPI). A matrix of NSP1, NSP2, and NSP3 prototypes and control substrates were submitted to Island Interferometry for scanning CPPI measurements that provide separate surface and bulk absorption data. The purpose of the testing is to determine if surface absorption depends on deposition sequence (NSP1 vs. NSP2), to understand if surface absorption increases for films deposited over nano-structure arrays, and to correlate the surface absorption measurements with laser damage testing.

The typical data set returned from CPPI measurements is illustrated in Figure 15. As shown by the inset diagram, the optic under test is moved through a focused 1064nm wavelength pump beam (2.5-2.9 Watts) that heats the material at the focus causing a spatial distortion that is sensed through self interference of a probe beam passing through the same spot. The overlap area is about 0.04mm and the scan step size is 0.02mm. A scan over 5mm records the absorption throughout the bulk and at both surfaces of the 4mm thick NSP windows. Sample NSP1-027 shown as the dashed gold curve is a control sample with a grating etched in the front surface and the back surface untreated, or in the as-polished condition. As the probe passes the front surface we see increased absorption to the 10-12 ppm/cm level that is typical of Corning 7980 UV fused silica. There are no spikes in absorption at either the front or the back surfaces indicating no surface absorption above the system noise floor - approximately 0.8 ppm for this fast scan setup. [The bulk ppm/cm measurement is converted to the surface ppm value by dividing by a factor of 22 for this setup geometry]. All of the samples tested had untreated back surfaces and barring any contamination should show no back surface signal. As further controls and to demonstrate various nano-micro structure functions that can be defined in fused silica surfaces without adding surface absorption, the additional all fused silica variants shown in Figure 16 were scanned and showed no surface signal.

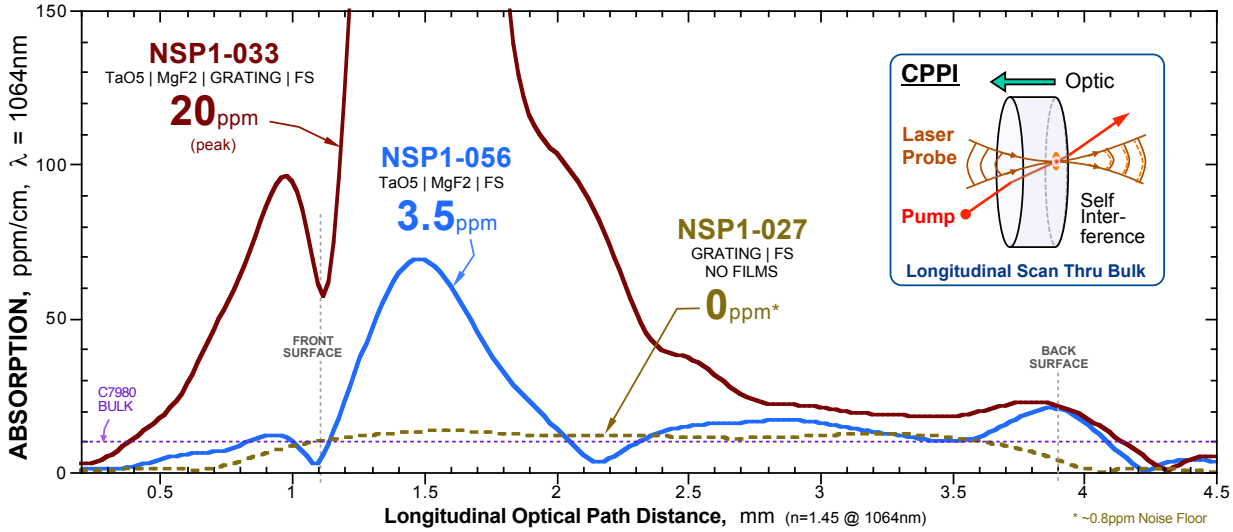

Figure 15: Absorption profile of fused silica windows at stages in the NSP1 fabrication sequence. Full prototype NSP1-033 (solid red curve), NSP1-056 with films only (solid blue curve), and NSP1-027 (dashed gold), a grating only with no films.

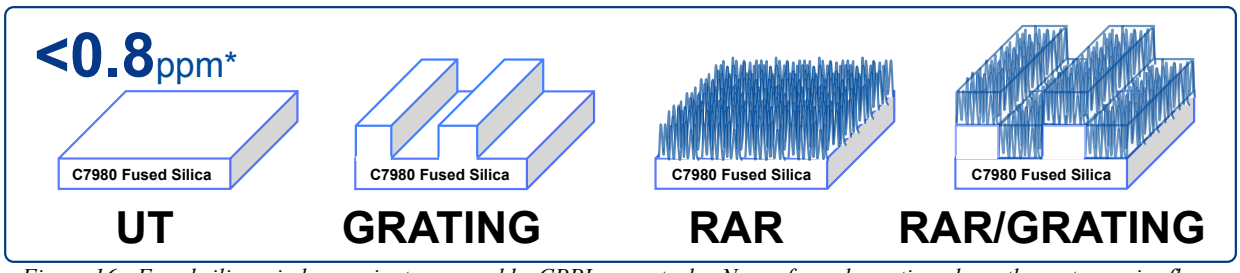

Figure 16: Fused silica window variants scanned by CPPI as controls. No surface absorption above the system noise floor.

Sample NSP1-056 (solid blue curve) of Figure 15 is intended to show the absorption of the Ta_2O_5 and MgF_2 films deposited on polished surfaces. About 3.5ppm absorption from the films is observed as the ~75ppm/cm peak at the front surface. Surprisingly, when the two film layers were deposited over the grating surface as with NSP1-033 (solid red curve) in Figure 15, the surface absorption increased dramatically to the 20ppm level. This absorption increase is also seen for the NSP2 and NSP3 designs and is summarized in Figure 17. The explanation for this is likely the film deposition defects described above.

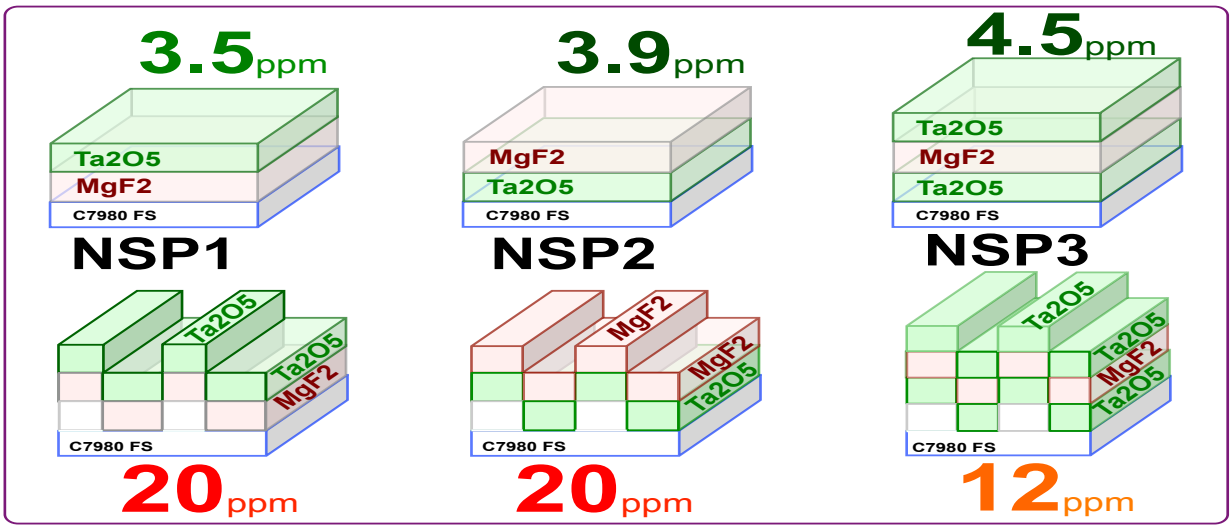

Figure 17: Surface absorption values for NSP1, NSP2, and NSP3 fused silica window variants scanned by CPPI.

4.0 PULSED LASER DAMAGE TESTING, 1064nm, 6.2ns

A set of 23 fused silica windows consisting of NSP1, NSP2, and NSP3 prototypes and control substrates were submitted to Lumibird (formerly Quantel USA) in Bozeman Montana for their commercial 's-on-1' type pulsed laser induced damage threshold measurements. "Damage" is defined as any permanent surface change that can be observed at high magnification (150x), and "threshold" is used to describe the lowest fluence required to induce damage at any site. Lumibird's testing adheres to the ISO 11254 standard and involves irradiating a test sample at several different fluence levels, multiple sites per fluence level. This protocol provides a quick look at damage resistance under high fluence and how LiDT correlates with absorption. The percentage of failures is plotted against the fluence levels, to which a least squares linear fit is applied. The 0% damage intercept of the fit determines overall threshold fluence. The specific test configuration was: Nd:YAG laser operating at 1064nm wavelength, 6.2ns pulse width (FWHM), 20Hz pulse repetition rate, 0.4-0.51mm focused spot diameters ($1/e^2$), TEM_{00} spatial mode, linear polarization, normal incidence illumination, ~100 exposure sites on a grid with spacing >2x spot diameter, 150 shots per site, 10 fluence levels. It is common in fused silica and other glasses under test to observe large scale back surface damage, or blow outs. Often this backside damage occurs without damage to the expose surface and is therefore not included in the damage count.

Figure 18 is a plot of this damage frequency as a function of fluence level for an NSP1 prototype (solid red diamond markers), along with a control sample consisting of a fused silica substrate with the Ta_2O_5 and MgF_2 film layers only – no grating (open blue square-X markers). Diagrams of each sample variant are inset in the Figure, and a linear fit for each data set is shown by the solid lines. The threshold for damage, the highest fluence for which no damage is observed at all sites, was found to be 7.4 J/cm^2 for the uniform film layer control sample, but only 2.7 J/cm^2 for the full NSP1 prototype. Such a low value was unexpected and may be related to the increased absorption and the coating growth defects discussed previously. The same trend of decreased pulsed LiDT for films deposited over gratings was seen with the NSP2 prototype as given in Figure 19. Interestingly the NSP3 design does not show this trend toward decreased LiDT, but this may be due to the near planarization of the NSP3 films as deposited, the large shift in spectral reflection toward shorter wavelengths, and the surface absorption increase was less than with the NSP1 and NSP2 prototypes.

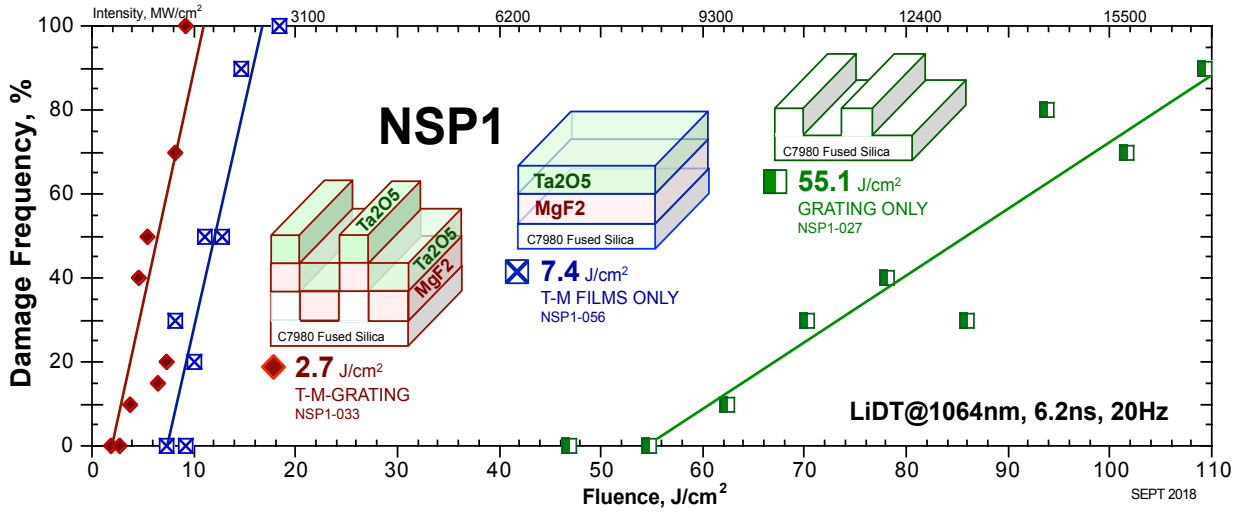

Figure 18: Pulsed laser induced damage frequency as a function of exposure fluence for a full NSP1 prototype (solid red diamond markers), a film only control sample (open blue square-X), and a grating only control (half filled green squares)

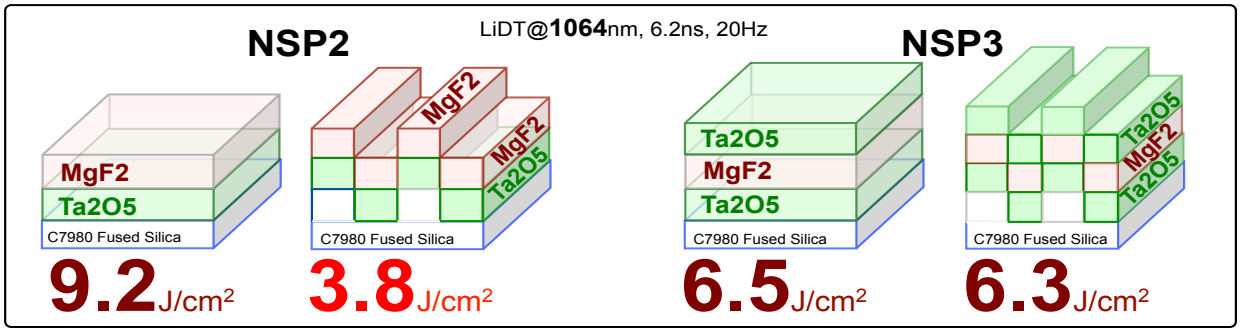

Figure 19: Diagrams and the pulsed LiDT of NSP2 and NSP3 prototypes and the corresponding film only control samples.

Also shown in Figure 18 is the pulsed LiDT of an additional control sample consisting of a grating only etched in the surface of a fused silica substrate – the first step in the NSP1 fabrication process prior to deposition of the Ta_2O_5 and MgF_2 film layers (half filled green square markers). The CPPI measurements of Figure 16 demonstrated that these gratings could be fabricated without adding surface absorption. The damage threshold is quite high at 55.1 J/cm^2, and the damage frequency data is well behaved indicating a uniform grating surface with a low defect count. High thresholds are also found for other samples of fused silica structures such as the Random AR (RAR) nano-texture and the RAR nano-texture superimposed on a grating structure as depicted in Figure 20. These all silica structures consistently exhibit pulsed laser damage thresholds between 3 and 10 times higher than any type of thin-film coating.

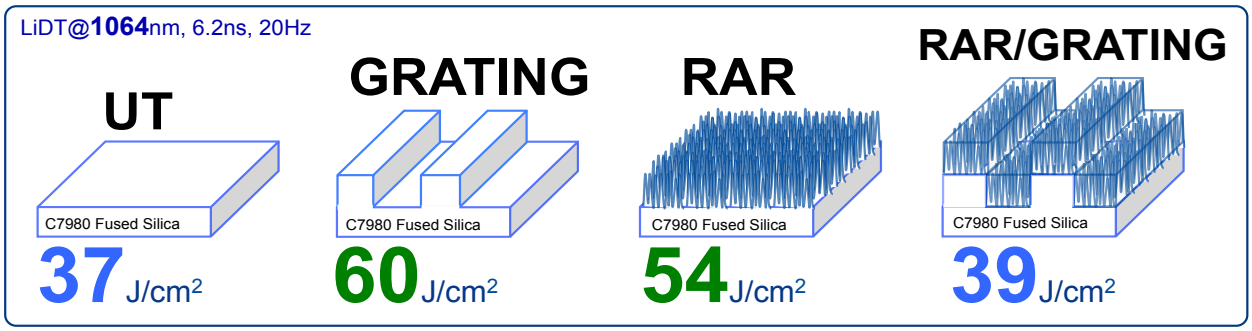

Figure 20: Diagrams of fused silica sample variants with various micro- and nano-structures etched in the surface – and no additional film layers. The exceptionally high pulsed LiDT values listed are well correlated to the lack of surface absorption.

5.0 SUMMARY

A continued study of nano-structure resonant polarizers was conducted with the goal of determining the fabrication methods that allow for reduced surface absorption, lower electric field enhancement, and increased laser damage resistance for high reflector and filter optics operating within high power laser systems. NSP prototypes based on gratings etched in fused silica and over-coated with tantala and magnesium fluoride films, exhibited >99.7% reflectivity for linearly polarized illumination over a several nm bandwidth with high transmission of the orthogonal polarization leading to extinction ratios greater than 300:1. Deviations in the measured NSP prototype performance from the model predictions were linked to film deposition issues such as reduced tantala refractive index and growth defects in the evaporated films. Surface absorption measurements showed an unexpected jump in surface absorption for films deposited over gratings compared to the same films deposited on polished surfaces. SEM revealed voids and lateral growth of the film layers that did not replicate the grating structure in the film layers. Pulsed laser damage testing at a wavelength of 1064nm with a 6.2ns pulse width also showed a reduced damage resistance for NSP prototypes compared to the films deposited on non-structured control substrates. Further work is ongoing to alter the deposition configuration in order to replicate the grating structure to better match the model structures.

6.0 ACKNOWLEDGEMENTS

The authors gratefully acknowledge the detailed surface and bulk absorption scans conducted by Chris Franz of Island Interferometry, a spin-out from Stanford PhotoThermal Solutions, Incorporated. Gary Shafer of Lumibird (GShafer@quantelusa.com) is also gratefully acknowledged for his fast and thorough work providing the certified, NIST traceable pulsed LiDT testing at 1064nm. The authors thank Tyler Wozmak & John Knowles at MicroVision Laboratories, Chelmsford MA for the detailed SEM images presented. Last, the authors greatly appreciate the helpful discussions with Karl George Jr. and the exceptional thin film dielectric coating services provided by his company Quality Thin Films, Inc. of Oldsmar Florida USA.

7.0 REFERENCES

[1] Lowdermilk, W. H., Milam, D., "Graded-index antireflection…., " Appl. Physics Letters, **36** (11), 891 (1980)
[2] Hobbs, D.S., MacLeod, B. D., "High laser damage…. micro-structures.., " Proc. SPIE, **6720**, 67200L (2007)
[3] Hobbs, D.S., et.al., "Contamination resistant antireflection nano-textures.., " Proc. SPIE, **8885**, 88850J (2013)
[4] Xin, Y., et. al., "High power laser antireflection subwavelength…, " J. Phys. D: Appl. Phys. **49**, 265104 (2016)
[5] Tolenis, T., et. al., "Sculptured anti-reflection coatings for high power…., " Opt. Mat. Exp. **7** (4), 1249 (2017)
[6] Hobbs, D.S., "Laser Damage Threshold Measurements... High Reflectors," Proc. SPIE **7132**, 71321K (2008)
[7] Pung, A., "High-power laser testing of 3D meta-optics, " Proc. SPIE, **8885**, 88850K (2013)
[8] Magnusson, R., "Wideband reflectors with zero-contrast gratings," Optics Letters **39,** (15) 4337 (2014)
[9] Chen, G., et. al., "Period photonic filters: theory and experiment, " Opt. Eng. **55** (3), 037108 (2016)
[10] Zhang, S., et. al., "Broadband guided-mode resonant reflectors with …. ," Opt. Exp. **25** (23), 28451 (2017)
[11] Hobbs, D.S., et. al., "Pulsed... nanostructured… reflectors… 355nm.., " Proc. SPIE, **10447**, 104470W (2017)
[12] Wang, S.S., and Magnusson, R., "Theory…. Guided-mode resonance filters, " Applied Optics **32**, 2606 (1993)
[13] COMSOL Multiphysics®, https://www.comsol.com/comsol-multiphysics
[14] Hobbs, D.S., et. al., "Automated Interference Lithography Systems for …..., " Proc. SPIE **3879**, 124 (1999)
[15] Tompkins, H.G. and Hilfiker, J.N., *Spectroscopic Ellipsometry: Practical Application to Thin Film Characterization*, New York: Momentum Press, (2016)
[16] Alexandrovski, A., et. al., "Photothermal common-path interferometry….." Proc. SPIE **7193**, 71930D (2009)